GI_Forum 2023, Issue 2
Page: 88 - 101
Full Paper
Corresponding Author:
kiarash.pooladsaz@stud.sbg.ac.at
DOI: 10.1553/giscience2023_02_s88

Monitoring the Evolution of the Kaiwhata Landslide in New Zealand using Object-based Image Analysis and Sentinel-2 Time Series

Kiarash Pooladsaz[1], Daniel Hölbling[1] and Jan Brus[2]

[1]University of Salzburg, Austria
[2]Palacký University Olomouc, Czechia

Abstract

Landslides are among the most serious geological hazards in mountainous and hilly areas of New Zealand, where they frequently cause significant damage and landscape changes. Monitoring the evolution of landslides and their consequences can help to mitigate hazards that could arise in later reactivation phases or in similar cases. The abundance of time-series remote sensing data has facilitated the mapping and monitoring of landslides. By applying object-based image analysis (OBIA) and using Sentinel-2 satellite data from 2017 to 2021, we aim to semi-automatically map the evolution of the Kaiwhata landslide and the subsequent impacts on the upstream area in the Wairarapa region in New Zealand. The OBIA mapping results revealed a gradual increase in the landslide area, with two major changes in June 2019 and November 2020. These major changes were followed by the formation of temporary landslide-dammed upstream lakes along the Kaiwhata river.

Keywords:

Landslide, Sentinel-2, Object-based Image Analysis (OBIA), landslide-dammed lake, New Zealand

1 Introduction

Natural hazards such as landslides can cause severe damage to infrastructure, human settlements and land (Alexander, 2005). A landslide (or 'landslide failure') is defined as the downward or outward displacement of debris (i.e. rock, soil and sediments) due to gravity (Cruden, 1991). A landslide can be triggered by natural events such as volcanic eruptions, earthquakes and intense rainfall, or human interventions, including road construction and land use changes (Hölbling et al., 2016). New Zealand's geomorphological characteristics provide ideal conditions for massive landslides, leading to costs of approximately $250 to $300 million a year (Rosser et al., 2017). The risk of landslides must not be ignored, not only because of the threat of damage to the immediate environment, but also because of potential knock-on incidents (Dabiri et al. 2020). Geomorphological features such as the Kaiwhata landslide can

block water courses, creating landslide-dammed lakes, resulting in a high level of risk for both the downstream and the upstream areas.

Compared to traditional field measurements, which are time-consuming and expensive (Abad et al., 2022), Earth Observation (EO) data have enabled more efficient monitoring of landslides and related hazard analysis. The now-multiple sources of optical imagery (including high-resolution (HR) and very high-resolution (VHR) satellite images, unmanned aerial vehicles (UAVs), synthetic aperture radar (SAR) data, and LiDAR data) can readily be drawn on in studies at different scales related to landslide recognition, inventory mapping, monitoring and change detection, susceptibility mapping, landslide volume estimation and so on (Mondini et al., 2021; Guzzetti et al., 2012; Xun et al., 2022; Hölbling et al., 2017; Karantanellis et al., 2020; Pawłuszek et al., 2019). The abundance of available satellite data highlights the value of EO data in enabling a better understanding of landslides, including their distribution, size and type, and facilitates time-series analysis of subsequent changes and the extent of damage (Hölbling, 2022).

Developments in remote sensing, and semi-automated and automated image analysis have improved the possibility of mapping landslides with less human interaction (Amatya et al., 2021). Object-based image analysis (OBIA) mimics human perception by aggregating a set of pixels into meaningful objects with defined homogeneity (Blaschke, 2010). OBIA demonstrates advantages over pixel-based approaches for mapping the extent, types and distribution of complex natural features such as landslides, which consist of twisted textures and extreme spectral heterogeneity (Hölbling et al., 2015). Landslide characteristics are not limited to their spectral signatures, and their topographic, morphological and contextual features must also be considered (Martha et al., 2010). The advances in OBIA stem from the multi-scale integration of spectral information (colour), spatial properties (e.g., size, shape), textural data (e.g., surface disturbance difference), and contextual information (e.g., relationship with neighbouring objects) (Blaschke et al., 2014). Used in conjunction with other datasets, such as a Digital Elevation Model (DEM) and its derivatives, OBIA has provided promising results in landslide mapping and change analysis (Hölbling, 2022; Martha et al., 2016; Blaschke et al., 2014; Amatya et al., 2021; Karantanellis et al., 2020). With these considerations in mind, this study aims to analyse the evolution of the Kaiwhata landslide and its impacts on the landscape in Wairarapa, New Zealand, using semi-automated OBIA and time series of Sentinel-2 images from 2017 to 2021.

2 Study Area

The study area is located in the south of New Zealand's North Island, in the Wairarapa region, east of Wellington (Figure 1). It covers 9.7 km² and is characterized by the Kaiwhata River, which flows southeast to the Pacific Ocean. The topography of the study area ranges from 10m to 500m a.s.l. It is covered mainly by grassland and forest, and is accessed by the Kaiwhata road.

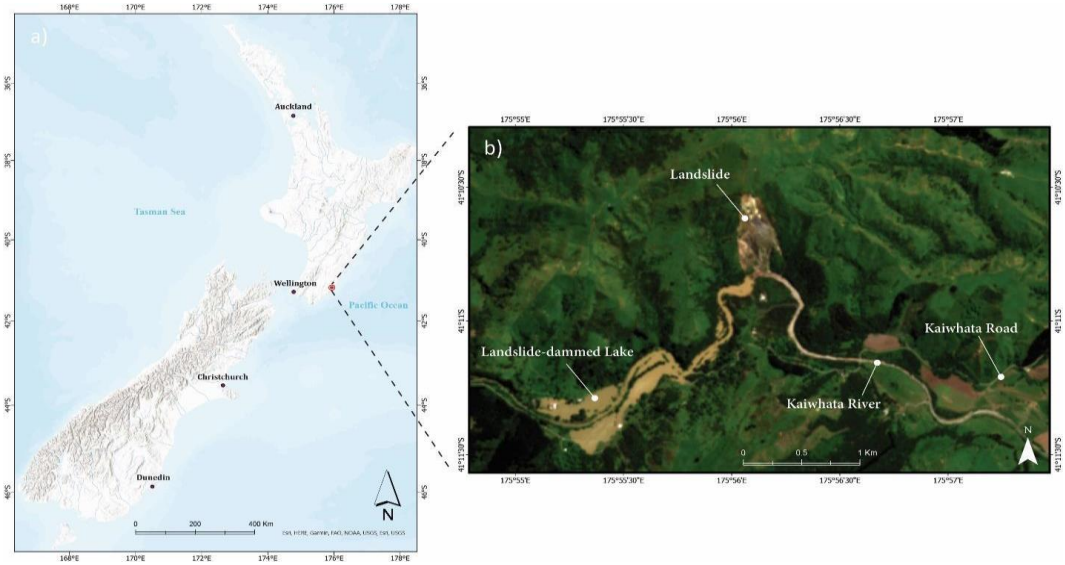

Figure 1: (a) Location of the study area in the south of North Island, New Zealand (background data: © ESRI); (b) Study area seen in a Sentinel-2 satellite image from 11 November 2020.

The initial landslide failure that occurred in 2017 in the Kaiwhata valley was comparatively small. The second, in June 2019 (Figure 2), was significantly larger. According to Morgenstern et al. (2021), the debris formed a dam, which lasted approximately two weeks, created an extensive upstream lake, and closed the Kaiwhata road. Due to the rising level of the lake, which overtopped the dam, the formation of a minor water channel flowing down the valley, and the types of material that had accumulated, the dam failed, releasing around 1.1 million m³ of water in less than two hours to the area downstream (Morgenstern et al. 2021).

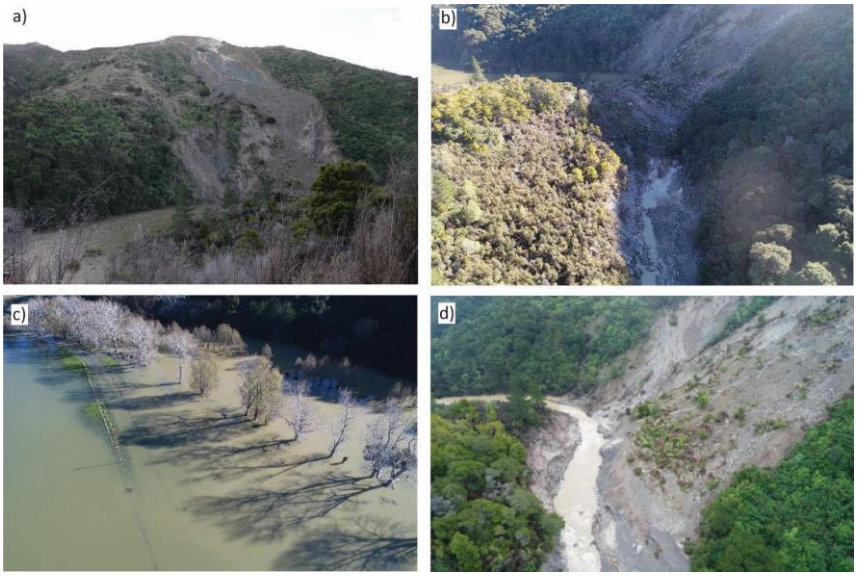

Figure 2: (a) South-to-north view of the second landslide failure (photograph: © B. Rosser; June 2019); (b) the landslide formed a dam and blocked the river (photograph: © R. Morgenstern; June 2019); (c) a lake was formed upstream and flooded the land and infrastructure (photograph: © R. Morgenstern; June 2019) (Rosser, 2019a); (d) the dam failed and an enormous amount of water was released (Rosser, 2019b)(photograph: © R. Morgenstern; June 2019).

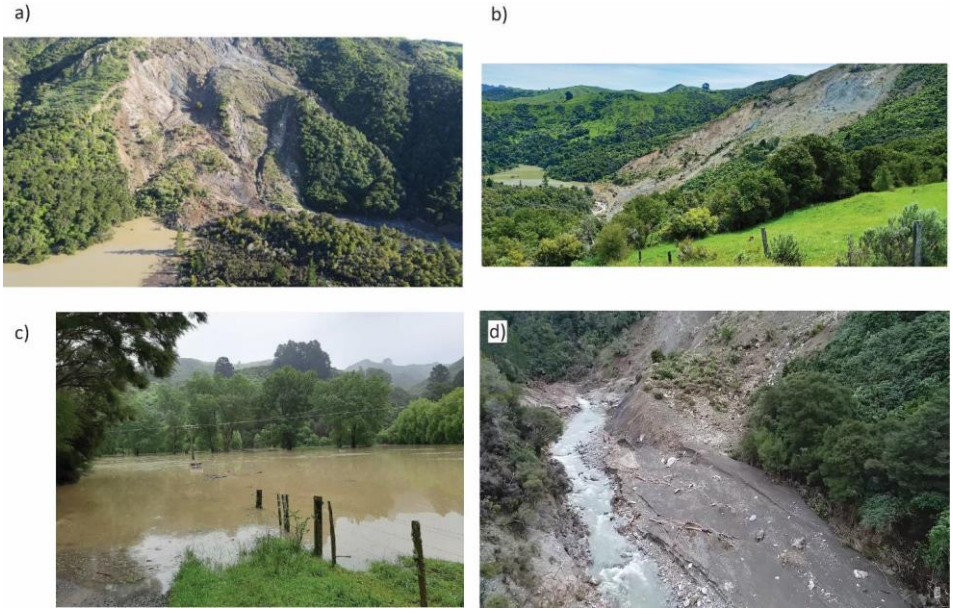

Figure 3: (a) South-to-north view of the third landslide failure (photograph: © M. Anselm; November 2020); (b) the landslide formed a dam and blocked the river (the landslide-dammed lake is visible on the left) (photograph: © Lithofile; November 2020); (c) a lake was formed upstream and flooded the land and infrastructure (photograph: © M. Anselm; November 2020); (d) the dam failed and an enormous amount of water was released (photograph: © GNS; December 2020).

The cycle repeated itself in November 2020 (Figure 3) when the landslide was reactivated after heavy rainfall, causing damage to adjacent properties, lands, the main road and other infrastructure (Anselm, 2020). Subsequently, the landslide-dammed lake overtopped the dam, and the dam failed.

3 Data

3.1 Optical Satellite Data

The satellite images used in this study cover a series of Kaiwhata landslide events and evolutions from 2017 to 2021. We used a time series of Sentinel-2 images with 10m spatial resolution and Red, Green, Blue (RGB) and Near-infrared (NIR) bands. In addition, we used one PlanetScope satellite image, provided by Planet, with four spectral bands (RGB and NIR) and 3m spatial resolution (Table 1). We used the PlanetScope image because there was no available Sentinel-2 image with low cloud coverage showing the significant changes for the desired date (between 1st and 13th of June 2019). We selected the images based on visual inspection; changes could be seen by comparing the images from the different dates recognized compared to the previous date; cloud cover was taken into consideration.

Table 1: Satellite images used for the analysis

Sensor, Product	Date	Event Description
Sentinel-2B MSI, Level 1-C	13 October 2017	First Landslide Failure
Sentinel-2B MSI, Level 1-C	16 January 2018	
Sentinel-2A MSI, Level 1-C	13 September 2018	
Sentinel-2A MSI, Level 1-C	12 November 2018	
PlanetScope MSI	8 June 2019	Second Landslide Failure
Sentinel-2A MSI, Level 1-C	18 September 2019	
Sentinel-2B MSI, Level 1-C	12 December 2019	
Sentinel-2A MSI, Level 1-C	11 November 2020	Third Landslide Failure
Sentinel-2A MSI, Level 1-C	1 December 2020	
Sentinel-2B MSI, Level 1-C	15 January 2021	

3.2 Topographic Data

The Land Information New Zealand (LINZ) Data Service provides open-source topographic and cadastral data, in addition to various other datasets. Through this platform, we acquired the Wellington region DEM with 1m spatial resolution, derived from LiDAR data from 2013 and 2014. Although the available data do not cover the overall timeframe of interest, the DEM and its derivatives, such as slope and aspect, were inserted as auxiliary data and helped to distinguish landslide and landslide-dammed lake areas from other areas.

4 Methodology

OBIA was applied to semi-automatically map the Kaiwhata landslide on each Sentinel-2 and PlanetScope image. In this context, 'semi-automatic approach' refers to a process that involves a combination of automated and manual steps to analyse image data (Blaschke, 2010). It entails using computer algorithms to automatically segment an image into meaningful objects and to define classification parameters based on expert knowledge and visual interpretation. The analyses were executed using eCognition (Trimble) software. The workflow consisted of multi-scale segmentation and knowledge-based classification rules to map the landslide and the landslide-dammed lake on each image. The classification rules and parameters were developed continuously from the first image to the subsequent ones, following the evolution of the landslide and the landslide-dammed lake area themselves.

In the first step, the normalized difference vegetation index (NDVI), normalized difference water index (NDWI), soil-adjusted vegetation index (SAVI), and brightness layer were calculated. Next, we applied multi-resolution segmentation (Baatz & Schäpe, 2000) to create image objects as the basis for classification. The scale parameter and homogeneity criteria (shape vs. colour, compactness vs. smoothness) define the size and shape of the image objects. The segmentation parameters were determined based on expert trial and error and visual assessment of the image objects, and taking the spatial resolution of the images into consideration (Table 2).

Table 2: Segmentation and classification parameters used for object-based landslide and landslide-dammed lake mapping

Event Description	Data	Class	Parameters for Multiresolution Seg2mentation	Layers for Segmentation	Main Classification Parameters
First Landslide Activity	Sentinel-2 (13 October 2017)	Landslide	Scale Parameter: 250; Shape criterion: 0.1; Compactness criterion: 0.4	blue, green, red, NIR, brightness	NDVI < 0.5 DEM > 200
	Sentinel-2 (16 January 2018)	Landslide	Scale Parameter: 250; Shape criterion: 0.1; Compactness criterion: 0.4	blue, green, red, NIR, brightness	NDVI < 0.45 DEM > 195
	Sentinel-2 (13 September 2018)	Landslide	Scale Parameter: 250; Shape criterion: 0.1; Compactness criterion: 0.4	blue, green, red, NIR, brightness	NDVI < 0.45 DEM > 195 Slope > 24 Aspect < 185

	Sentinel-2 (12 November 2018)	Landslide	Scale Parameter: 250; Shape criterion: 0.1; Compactness criterion: 0.4	blue, green, red, NIR, brightness	First Part: NDVI < 0.5 DEM > 190 Second Part: NDVI < 0.5 Mean Slope > 30 DEM > 30 Mean Aspect < 190 Relative Border First Border = 0 Mean Brightness > 1000 Distance to First Part < 0.5 km
Second Landslide Activity	PlanetScope (8 June 2019)	Landslide	Scale Parameter: 50; Shape criterion: 0.3; Compactness criterion: 0.6	blue, green, red, NIR, brightness, NDVI, SAVI	NDVI < 0.5 DEM > 30 Slope > 24 Aspect < 201 SAVI < 0.7
		Landslide-dammed Lake	Scale Parameter: 25; Shape criterion: 0.1; Compactness criterion: 0.4	NDWI, DEM, slope	NDVI < 0.5 NIR < 1300 NDWI > -0.5
	Sentinel-2 (18 September 2019)	Landslide	First part: Scale Parameter: 250; Shape criterion: 0.1; Compactness criterion: 0.4 Second part: Scale Parameter: 10; Shape criterion: 0.1; Compactness criterion: 0.4	blue, green, red, NIR, brightness NDVI, NDWI	NDVI < 0.5 DEM > 30 Slope > 24 Aspect < 201 Mean Brightness > 700 NDVI < 0.3 NDWI < 0 Slope < 24 DEM < 200 Relative Border to First part > 0.25
	Sentinel-2 (12 December 2019)	Landslide	First part: Scale Parameter: 250; Shape criterion: 0.1; Compactness criterion: 0.4	blue, green, red, NIR, brightness	NDVI < 0.5 DEM > 30 Slope > 24 Aspect < 225 Mean Brightness > 700

			Second part: Scale Parameter: 10; Shape criterion: 0.1; Compactness criterion: 0.4	NDVI, NDWI	NDVI < 0.3 NDWI < 0 Slope < 24 DEM < 200 Relative Border to First part > 0.25
Third Landslide Activity	Sentinel-2 (11 November 2020; 1 December 2020; 15 January 2021)	Landslide	First part: Scale Parameter: 250; Shape criterion: 0.1; Compactness criterion: 0.4	blue, green, red, NIR, brightness	NDVI < 0.5 DEM > 30 Slope > 24 Aspect < 225 Mean Brightness > 700
			Second part: Scale Parameter: 10; Shape criterion: 0.1; Compactness criterion: 0.4	NDVI, NDWI	NDVI < 0.3 NDWI < 0 Slope < 24 DEM < 200 Relative Border to First part > 0.25
		Landslide-dammed Lake	Scale Parameter: 10; Shape criterion: 0.1; Compactness criterion: 0.4	NDWI, DEM, slope	NDVI < 0.5 NIR < 1300 NDWI > -0.5

For segmentation of the landslide area, we used the four multispectral bands and the brightness layer. Since the characteristics of the deposition zone of the landslide area and the riverbed were similar, we executed another segmentation on the unclassified objects to create homogeneous objects based on the NDWI and NDVI indices. This helped us to better map the total landslide area. We also applied a further segmentation on the unclassified objects for the landslide-dammed lake area based on the NDWI, the DEM and the slope.

The knowledge-based classification was based mainly on the spectral indices calculated. The main feature of the landslide area is the absence of vegetation. Such landslide-affected areas can be distinguished from their surroundings by applying spectral indices such as NDVI and the brightness layer. We also used the relatively low NDWI value to distinguish the deposition area of the landslide from the riverbed. For the mapping of the lake area, we applied relatively low near-infrared and NDVI values, and higher NDWI values. The DEM and its derivatives were used as auxiliary data to avoid the classification of false positives – for example, to distinguish the landslide area from the riverbed. The classification parameters and values were assigned based on expert knowledge, information from the literature, and trial and error.

5 Results and Discussion

5.1 OBIA Landslide Mapping

The results of the semi-automatically mapped Kaiwhata landslide and landslide-dammed lake areas are shown in Figure 4. The figure shows the significant changes in the landslide area, the formation of the landslide-dammed lake, and the changes in the lake area during the landslide evolution. The PlanetScope image for 8 June 2019 used in the analysis is visualized as a false-colour image to better show the flooded area. Most of the landslide area is covered by shadows during the summer, due to its particular topography.

The images from 2017 and 2018 reflect slight changes in the extent of the initial landslide, showing how it evolved continuously. The landslide was activated in two separate but adjacent areas. Over time, these areas evolved and the vegetation between them became more sparse. The image from 16 January 2018 shows that the two separate landslides had reached each other; however, vegetation persisted between the adjacent parts and we excluded it from the landslide. The vegetated area had diminished in the image from 13 September 2018 and the landslide had become relatively unmixed. The topographic features of the area and the precipitation created two streams of water from the upper part, which caused erosion and incision, resulting in new small landslips that are visible in the image from 12 November 2018. The erosion continued over time and destabilized the entire slope, probably leading to the second landslide failure.

The second landslide failure, in summer 2019, resulted in the formation of a landslide-dammed lake, because the debris flow reached the Kaiwhata riverbed and blocked the stream. The main landslide expanded and merged into the smaller ones. According to Morgenstern et al. (2021), intense rainfall triggered the landslide and hence created the landslide-dammed lake, which existed for two weeks. This scenario also occurred in 2020, with a third landslide failure and a larger lake, which this time persisted for more than six weeks until the dam failed. Figure 5 presents information regarding the evolution of the Kaiwhata landslide and the landslide-dammed lake area for each date.

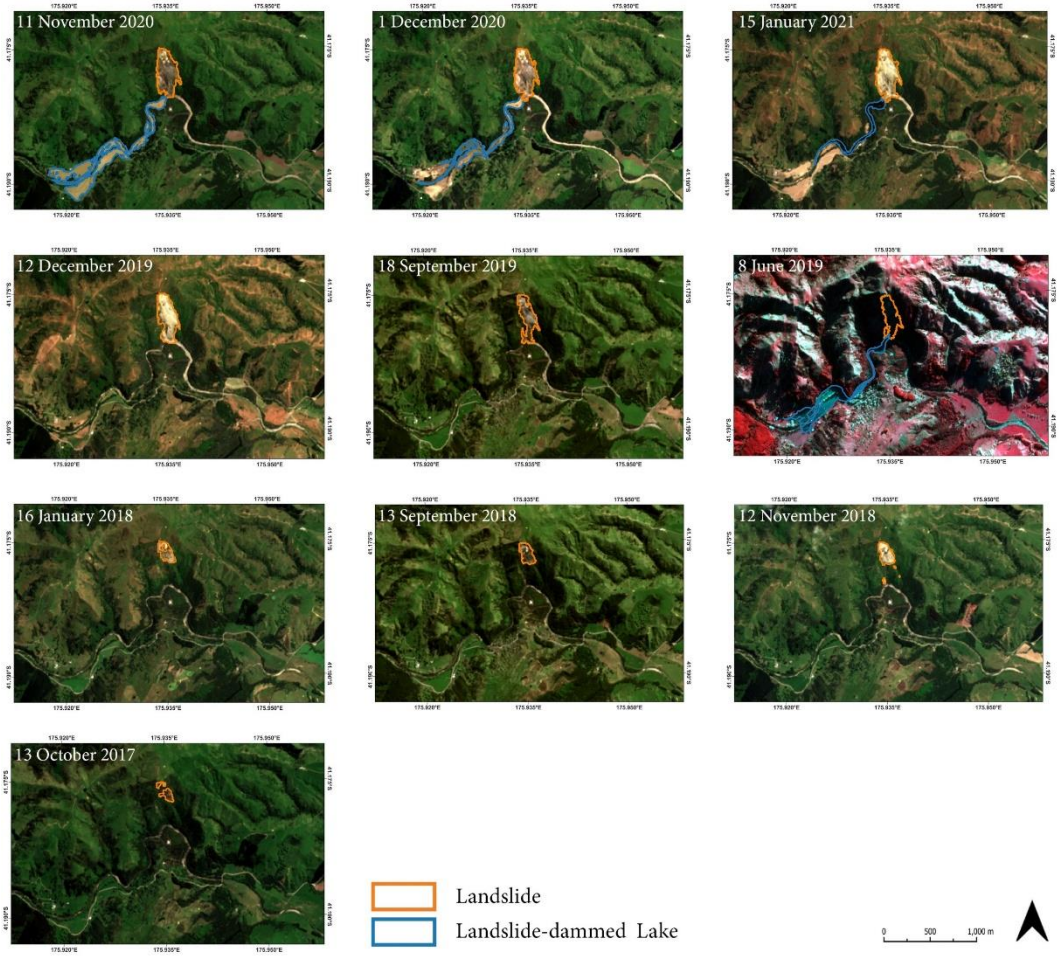

Figure 4: OBIA landslide mapping results for Kaiwhata, showing the evolution of the landslide from 2017 to 2021, and the landslide-dammed lake detected in 2019 and 2020.

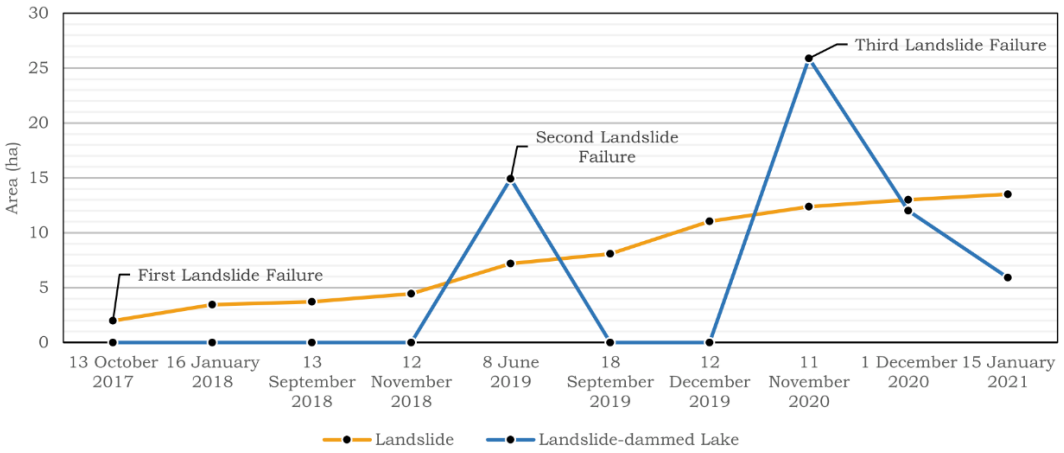

Figure 5: Time series showing the evolution of the Kaiwhata landslide and landslide-dammed lake.

5.2 Validation

The semi-automated OBIA results were compared with the results from the visual interpretation to assess the accuracy of the mapped areas. To do this, we performed a comparison of all results but chose mainly the images that highlight significant differences between OBIA and manual digitization. To validate the landslide and landslide-dammed lake areas, manual digitization was performed at a scale of 1:10,000. The producer's accuracy was calculated by dividing the overlap area by the area of the reference data (i.e., the manual mapping result); the user's accuracy was calculated by dividing the overlap area by the OBIA mapping result.

Table 3: OBIA and manual mapping (MM) results, the difference between OBIA and MM results, overlapping area, and producer's and user's accuracies for the selected image.

Image	Class	OBIA Mapping (ha)	Manual Mapping (ha)	Difference OBIA-MM (%)	Overlap Area (ha)	Producer's Accuracy (%)	User's Accuracy (%)
13 October 2017	Landslide	1.98	2.21	- 10.41	1.84	83.25	92.92
12 November 2018	Landslide	4.45	4.24	4.72	3.94	92.92	88.53
8 June 2019	Landslide	7.20	7.10	1.39	6.50	91.54	90.27
	Landslide-dammed Lake	14.91	19.76	- 24.55	13.45	68.09	90.20
11 November 2020	Landslide	12.29	12.58	- 2.31	12.04	95.7	97.96
	Landslide-dammed Lake	25.88	32.73	- 20.92	24.28	74.18	93.81

15 January 2021	Landslide	13.32	13.67	- 2.57	12.66	92.61	90.54
	Landslide-dammed Lake	5.76	5.05	12.24	4.55	90.09	78.99

The producer's and user's accuracies for the landslide and landslide-dammed lake areas resulted in different values. The mixture of sparse vegetation and the landslide area, and the uncertain border between the landslide and the lake, influenced the validation results. Moreover, the subjectivity inherent in manual interpretation may have influenced the accuracy values.

The largest difference between OBIA and manual mapping for the landslide relates to the image from 13 October 2017. The high user's accuracy value on this date confirms the assumption that manual mapping includes larger areas. This is why the producer's accuracy related to this date is the lowest. The values related to 12 November 2018 show that the producer mapped a larger extent than our semi-automatically delineated areas and ignored the small, separated landslips. This is why the producer's accuracy is much higher than the user's accuracy. The lower producer's accuracy for the landslide-dammed lake on 8 June 2019 and 11 November 2020 results from the existence of dense vegetation along the river. These are the dates when the lake reached its greatest extent, and the mixture of vegetation and water was relatively high. The manual delineation identified vegetated areas mixed with flooded areas as landslide-dammed lake. The OBIA mapping excluded vegetated areas because of their high NDVI and low NDWI values and their rather large extent. This indicates that the manual reference shows a degree of generalization. Thus, the comparison between OBIA results and manual mapping should be considered with caution because any manual reference data comes with a certain degree of uncertainty.

6 Conclusion and Outlook

OBIA allows the integration of abundant satellite images with topographic data, guided by explicit knowledge, to achieve customized classification results. This technique offers an efficient toolset to semi-automatically map the evolution of landslides, although few researchers have applied OBIA to analyse a time series of satellite images to monitor the evolution of a major landslide. Our workflow was designed to be transferable to all the images used and adaptive to landslide evolution. Consequently, only minor modifications were required to address the complexity of the landslide mapping. Applying multiresolution segmentation using different image layers and spectral indices in multiple steps allowed us to reach high classification accuracies. We used mainly spectral indices with the support of DEM data and its derivatives to classify the landslide and landslide-dammed lake areas. The DEM data helped to remove false classifications, despite the fact that the DEM shows the pre-landslide status of the terrain.

The Sentinel-2 satellite time-series images provided us with suitable material to analyse the evolution of the Kaiwhata landslide and landslide-dammed areas. Following the second landslide, cloud cover (a general problem with optical imagery) limited the choice of the most suitable images for change-identification. In addition, the topography of the area and the angle

of the sun during spring and summer limited the acquisition of shadow-free images. Several studies have demonstrated the suitability of synthetic aperture radar (SAR) data, such as Sentinel-1 data, for landslide mapping and analysis (Dabiri et al., 2020; Xun et al., 2022). Therefore, complementing the OBIA workflow with Sentinel-1 data in future studies could help address the area's probable landscape changes more efficiently.

Landslides in New Zealand, triggered by rainfall, snowmelt and earthquakes, often result in significant landscape changes (Korup, 2004). Our study revealed the gradual changes over time to both the landslides themselves and the areas around them. Future research should assess the possible correlation between heavy precipitation and landslide reactivation over time.

Acknowledgements

This research has been partly supported by the New Zealand Ministry of Business, Innovation and Employment (MBIE) through the project STEC ('Smarter Targeting of Erosion Control'; Contract C09X1804).

References

Abad, L., Hölbling, D., Spiekermann, R., Prasicek, G., Dabiri, Z., & Argentin, A. L. (2022). Detecting landslide-dammed lakes on Sentinel-2 imagery and monitoring their spatio-temporal evolution following the Kaikōura earthquake in New Zealand. Science of the Total Environment, 820, 153335. doi.org/10.1016/j.scitotenv.2022.153335

Alexander, D. (2005). Vulnerability to landslides. Landslide hazard and risk, 175-198. doi.org/10.1002/9780470012659.ch5

Amatya, P., Kirschbaum, D., Stanley, T., & Tanyas, H. (2021). Landslide mapping using object-based image analysis and open source tools. Engineering geology, 282, 106000. doi.org/10.1016/j.enggeo.2021.106000

Anselm, M. (2020) Properties under Treat after Landslide. Retrieved from https://www.rnz.co.nz/news/ldr/430482/properties-under-threat-after-landslide

Baatz, M., & Schäpe, A. (2000). Multiresolution Segmentation: an optimization approach for high quality multi-scale image segmentation.

Blaschke, T. (2010). Object based image analysis for remote sensing. ISPRS journal of photogrammetry and remote sensing, 65(1), 2-16. doi.org/10.1016/j.isprsjprs.2009.06.004

Blaschke, T., Hay, G. J., Kelly, M., Lang, S., Hofmann, P., Addink, E., ... & Tiede, D. (2014). Geographic object-based image analysis–towards a new paradigm. ISPRS journal of photogrammetry and remote sensing, 87, 180-191. doi.org/10.1016/j.isprsjprs.2013.09.014

Cruden, D. M. (1991). A simple definition of a landslide. Bulletin of the International Association of Engineering Geology-Bulletin de l'Association Internationale de Géologie de l'Ingénieur, 43(1), 27-29. doi.org/10.1007/BF02590167

Dabiri, Z.; Hölbling, D.; Abad, L.; Helgason, J.K.; Sæmundsson, Þ.; Tiede, D. Assessment of Landslide-Induced Geomorphological Changes in Hítardalur Valley, Iceland, Using Sentinel-1 and Sentinel-2 Data. Appl. Sci. 2020, 10, 5848. doi.org/10.3390/app10175848

GNS Science (2021) The Kaiwhata Landslide Dam. Retrieved from https://slidenz.net/theme-3/the-kaiwhata-landslide-dam/

Guzzetti, F., Mondini, A. C., Cardinali, M., Fiorucci, F., Santangelo, M., & Chang, K. T. (2012). Landslide inventory maps: New tools for an old problem. Earth-Science Reviews, 112(1-2), 42-66. doi.org/10.1016/j.earscirev.2012.02.001

Hölbling, D. (2022). Data and knowledge integration for object-based landslide mapping–challenges, opportunities and applications. gis. Science. Die Zeitschrift für Geoinformatik, 2022(1), 1-13.

Hölbling, D., Abad, L., Dabiri, Z., Prasicek, G., Tsai, T. T., & Argentin, A. L. (2020). Mapping and analyzing the evolution of the Butangbunasi landslide using Landsat time series with respect to heavy rainfall events during Typhoons. Applied Sciences, 10(2), 630. https://doi.org/10.3390/app10020630

Hölbling, D., Betts, H., Spiekermann, R., & Phillips, C. (2016). Identifying spatio-temporal landslide hotspots on North Island, New Zealand, by analyzing historical and recent aerial photography. Geosciences, 6(4), 48. https://doi.org/10.3390/geosciences6040048

Hölbling, D., Eisank, C., Albrecht, F., Vecchiotti, F., Friedl, B., Weinke, E., & Kociu, A. (2017). Comparing manual and semi-automated landslide mapping based on optical satellite images from different sensors. Geosciences, 7(2), 37. https://doi.org/10.3390/geosciences7020037

Hölbling, D., Friedl, B., & Eisank, C. (2015). An object-based approach for semi-automated landslide change detection and attribution of changes to landslide classes in northern Taiwan. Earth Science Informatics, 8(2), 327-335. https://doi.org/10.1007/s12145-015-0217-3

Karantanellis, E., Marinos, V., Vassilakis, E., & Christaras, B. (2020). Object-based analysis using unmanned aerial vehicles (UAVs) for site-specific landslide assessment. Remote Sensing, 12(11), 1711. doi.org/10.3390/rs12111711

Korup, O. (2004). Geomorphometric characteristics of New Zealand landslide dams. Engineering Geology, 73(1-2), 13-35. doi.org/10.1016/j.enggeo.2003.11.003

Lithofile (2020, November 27). Reactivated Landslide Dam. Kaiwhata River, New Zealand. [Online forum]. Retrieved from https://www.reddit.com/r/geomorphology/comments/k1xp51/reactivated_landslide_dam_kaiwhata_river_new/

Martha, T. R., Kamala, P., Jose, J., Vinod Kumar, K., & Jai Sankar, G. (2016). Identification of new landslides from high resolution satellite data covering a large area using object-based change detection methods. Journal of the Indian Society of Remote Sensing, 44(4), 515-524. doi.org/10.1007/s12524-015-0532-7

Martha, T.R., Kerle, N., Jetten, V.G., Westen, C.J., & Kumar, K.V. (2010). Characterising spectral, spatial and morphometric properties of landslides for semi-automatic detection using object-oriented methods. Geomorphology, 116, 24-36.

Mondini, A. C., Guzzetti, F., Chang, K. T., Monserrat, O., Martha, T. R., & Manconi, A. (2021). Landslide failures detection and mapping using Synthetic Aperture Radar: Past, present and future. Earth-Science Reviews, 216, 103574. doi.org/10.1016/j.earscirev.2021.103574

Morgenstern, R., Massey, C., Rosser, B., & Archibald, G. (2021). Landslide dam hazards: assessing their formation, failure modes, longevity and downstream impacts. Understanding and Reducing Landslide Disaster Risk: Volume 5 Catastrophic Landslides and Frontiers of Landslide Science 5th, 117-123. doi.org/10.1007/978-3-030-60319-9_12

Rosser, B. (2019a) Landslide Dam at Kaiwhata River. Retrieved from https://www.geonet.org.nz/news/3SF3C5Qz6k8MSGXmVUPDcn

Rosser, B. (2019b) Update on Landslide Dam at Kaiwhata River. Retrieved from https://www.geonet.org.nz/news/2qwgEidlRAVZWs5J0iUBvu

Rosser, B., Dellow, S., Haubrock, S., & Glassey, P. (2017). New Zealand's national landslide database. Landslides, 14(6), 1949-1959. doi.org/10.1007/s10346-017-0843-6

Xun, Z., Zhao, C., Kang, Y., Liu, X., Liu, Y., & Du, C. (2022). Automatic Extraction of Potential Landslides by Integrating an Optical Remote Sensing Image with an InSAR-Derived Deformation Map. Remote Sensing, 14(11), 2669. doi.org/10.3390/rs14112669